The calculation of turbulent swirling flow through wide angle conical diffusers and the associated dissipative losses

C. B. Okhio*, H. P. Horton† and G. Langer**

For turbulent swirling flow in a duct of circular cross-section, the time-averaged Navier-Stokes and continuity equations are written, and by introducing into these equations the longitudinal vorticity ω and stream-function ψ, they are cast in a form amenable to digital computer using well known finite difference techniques. A model of effective viscosity is introduced and the suitability of its various forms is discussed. The Van-Driest modification to the Prandtl mixing length concept is applied near the solid boundary while the model used far from the boundary is a simple form of the mixing length model. This simple model is found to provide realistic predictions when comparisons are made with available experimental mean axial velocity data for flow through a 16.5° conical diffuser (area ratio 4.4) fitted with a tailpipe.

Keywords: *turbulent swirling flow, digital computer, effective viscosity, mean axial velocity data*

The performance of a diffuser containing stall can be appreciably improved by reasonable levels of inlet swirl, but when the strength of the inlet swirl exceeds a certain threshold the flow in the diffuser is accompanied by a central recirculation zone. Both the circumferential velocity component and the central recirculating flow have the effects of convecting the main flow momentum and energy towards the wall, thereby counteracting the tendency of the flow to separate from the wall. Such a swirling flow may either be generated using a swirl generator, or it may be inherent in the nature of the installation.

The subject of swirling flow in wide angle diffusers appears to have received limited attention in the past. Various experimentalists (eg Refs 1–9) have adopted the empirical approach of constructing and testing the performance of numerous wide angle diffusers. Such an approach can be time consuming and may well be uneconomic. An alternative approach is to establish a reliable theoretical model to enable a rational design procedure to be carried out. In 1975, Al-Obaidi[10] carried out an experimental and theoretical study of the flow distribution in a 30° angle diffuser. The boundary layer method of calculation developed by Patankar and Spalding[13] was applied to his diffuser geometry. The main objective was to investigate whether a mixing-length model of turbulence would yield satisfactory results in the non-separated regions of the flow. The theoretical analysis yielded results in fair agreement with the experimental data in these regions. However, since a boundary layer analysis is not applicable in the region of flow separation due to the inherent nature of the boundary layer assumptions, a complete solution of the flow in a wide angle diffuser requires the use of the full Navier-Stokes equations.

Accordingly, in the present investigation, the full Navier-Stokes and continuity equations have been solved numerically for the time-mean flow by adapting the finite difference method of calculation developed by Gosman *et al*[11]. One of the main objectives was to investigate whether a mixing-length turbulence model would yield satisfactory agreement between calculated and experimental distributions of flow through diffusers including the region of flow separation. In addition, an experimental investigation into the flow in a wide angle diffuser was carried out. This is reported in the authors' previous work[15]. The diffuser was fitted with a tailpipe in order that the downstream boundary conditions used in the calculations should be a good approximation to those occurring in the experiment.

The method of calculation

The majority of fluid flow problems of practical interest are turbulent. In the flow of fluid through wide angle diffusers the influence of the laminar viscous layer is confined to the solid boundary. Turbulent flows are not amenable to exact analysis using existing mathematical methods, and the current engineering approach to the solution of turbulent flow problems is to solve a steady, time-averaged set of equations using suitable empirical assumptions to model certain terms in order to obtain a closed problem. The accuracy of the solution depends both on the validity of the empirical input and on the sophistication of the model, although the most

* Now of Faculty of Engineering and Technology, Bendel State University, PMB 14, Ekpoma
† Aeronautical Engineering Department, Queen Mary College, UK
** Now deceased of: Mechanical Engineering Department, Queen Mary College, UK
Received 12 September 1983, accepted for publication 5 September 1985

sophisticated models do not necessarily yield the best results.

Starting from the full Navier-Stokes equations and continuity equation in cylindrical-polar co-ordinates, suitable forms of the equations are established which make it possible to calculate parabolic and elliptic-type swirling turbulent flows.

In this investigation a quasi-cylindrical polar co-ordinate system based on a slightly non-orthogonal mesh has been used, so that the outer mesh points lie on the flow boundaries. To check the applicability of the chosen scheme we have calculated the flow distribution in a diffuser using both the scheme and an orthogonal polar co-ordinate scheme. A comparison of the two schemes' results has been made and we have observed that the non-orthogonal scheme seems more attractive because of its simplicity and flexibility, but it does not appear to have been much used.

The scheme is very convenient for obtaining solutions for flows in ducts of arbitrary shape, provided that the curvature of such duct boundaries is small when, as shown in the present author's previous results[15], the errors incurred are negligible. The approximations made would amount to an assumption of a quasi-1-D flow, apart from the influence of the viscous terms in the equations. The diffusers considered here are of small enough angles that the errors involved in the approximations are negligible for engineering purposes.

The classical procedure for describing turbulent flows mathematically entails separating the instantaneous flow parameters into their mean and fluctuating components, and for example in terms of the present notation, the instantaneous axial velocity component $U_z = \bar{U}_z + U'_z$, where $\bar{U}_z$ and U'_z are the mean and fluctuating constituents of U_z respectively. For 3-D cylindrical co-ordinates the Navier-Stokes equations are given in Goldstein[9] in terms of time-averaged and fluctuating components.

For the present situation treated as 2-D in the plane $z \sim r$, the directions z and r equations become:

$$U_z\frac{\partial U_z}{\partial z}+U_r\frac{\partial U_z}{\partial r}=-\frac{1}{\rho}\frac{\partial P}{\partial z}+\frac{1}{\rho}\frac{\partial}{\partial z}\left\{\mu\frac{\partial U_z}{\partial z}-\rho\overline{u_z'^2}\right\}+\frac{1}{\rho r}\frac{\partial}{\partial r}\left\{\mu r\frac{\partial U_z}{\partial r}-\rho r\overline{u'_z u'_r}\right\} \quad (1)$$

$$U_r\frac{\partial U_r}{\partial r}+U_z\frac{\partial U_r}{\partial z}-\frac{U_\theta^2}{r}=-\frac{1}{\rho}\frac{\partial P}{\partial r}+\frac{\partial}{\partial z}\left\{\mu\frac{\partial U_r}{\partial z}-\rho\overline{u'_z u'_r}\right\}+\frac{1}{\rho r}\frac{\partial}{\partial r}\left\{\mu r\frac{\partial U_r}{\partial r}-\rho r\overline{u_r'^2}\right\}-\left\{\mu\frac{U_r}{r^2}-\frac{\overline{u_\theta'^2}}{r}\right\} \quad (2)$$

and the continuity equation becomes:

$$\frac{\partial U_r}{\partial r}+\frac{U_r}{r}+\frac{\partial U_z}{\partial z}=0 \quad (3)$$

In modelling turbulent flows the concept of an effective viscosity μ_{eff} is adopted here, where

$$\mu_{\text{eff}}=\mu+\mu_t \quad (3a)$$

μ and μ_t being the laminar and turbulent viscosities

Notation

a_ϕ	A coefficient in the general elliptic equation
a_{UR}	The under-relaxation parameter
A_E, A_W, A_N, A_S	Coefficients in the convection terms of the difference equation
A'_j	A coefficient in the general substitution formula
b_ϕ	A coefficient in the general substitution formula
B_E, B_W, B_N, B_S	Coefficients in the diffusion terms of the difference equation
c_ϕ	A coefficient in the general elliptic equation
h	Height of grid line
I	Integer index denoting the streamwise direction
J	Integer index denoting the cross-stream direction
K	Mixing constant
$\dot{m}$	Mass flow rate
l	Mixing length
P	Pressure
S_N	Swirl number
τ	Shear stress
U_z, U_r, U_θ	Components of velocity vector in three orthogonal directions z, r and θ respectively
$\bar{U}$	Implies average velocity
U	Total velocity vector
U'	Instantaneous velocity
α	Swirl blade angle
β	Small angle less than one radian
ρ	Density of the fluid
μ	Laminar viscosity of the fluid
μ_{eff}	Effective viscosity of the fluid $(=\mu+\mu_t)$
μ_t	Turbulent viscosity of the fluid
ϕ	The dependent variable of the general elliptic equation
ψ	The stream function
ω	Vorticity
Σ_{AB}	A group of terms in the substitution formula
z, r, θ	Cylindrical coordinates
y	Distance from solid boundary

Subscripts

n, s, e, w	Pertaining to the co-ordinates of the sides of the 'tank'
c	Indicates centre-line
N. S. E. W	Refers to neighbouring nodes which lie respectively north, south, east and west of node P
NE, NS, NW, SW	Refers to nodes which lie near to nodes N, S, E and W
ω	Refers to the vorticity ω or ω/r

Superscripts

$\bar{}$	Indicates average value
$'$	Indicates instantaneous value

respectively. Analogous to the direct relationship between the viscous shear and mean velocity gradient, the turbulent shear stresses are obtained by replacing the laminar viscosity μ by $\rho\varepsilon$ where ε is the eddy viscosity thus:

$$\overline{\rho u_r' u_\theta'} = \rho\varepsilon\left(\frac{\partial U_\theta}{\partial r} - \frac{U_\theta}{r}\right) \tag{4}$$

$$\overline{\rho u_\theta' u_z'} = \rho\varepsilon\left(\frac{\partial U_\theta}{\partial z}\right) \tag{5}$$

$$\overline{\rho u_r' u_z'} = \rho\varepsilon\left(\frac{\partial U_r}{\partial z} + \frac{\partial U_z}{\partial r}\right) \tag{6}$$

The time-averaged Navier-Stokes equations and continuity equations then become:

$$U_r\frac{\partial U_r}{\partial r} + U_z\frac{\partial U_r}{\partial z} - \frac{U_\theta^2}{r} = -\frac{1}{\rho}\frac{\partial P}{\partial r} + \frac{\mu_{\text{eff}}}{\rho}\left(\frac{1}{r}\frac{\partial}{\partial r}\left(r\frac{\partial U_r}{\partial r}\right) + \frac{\partial^2 U_r}{\partial z^2} - \frac{U_r}{r^2}\right) \tag{7}$$

$$U_r\frac{\partial U_z}{\partial r} + U_z\frac{\partial U_z}{\partial z} = -\frac{1}{\rho}\frac{\partial P}{\partial z} + \frac{\mu_{\text{eff}}}{\rho}\left(\frac{1}{r}\frac{\partial}{\partial r}\left(r\frac{\partial U_z}{\partial r}\right) + \frac{\partial^2 U_z}{\partial z^2}\right) \tag{8}$$

$$\frac{\partial U_r}{\partial r} + \frac{U_r}{r} + \frac{\partial U_z}{\partial z} = 0 \tag{9}$$

where $\mu_{\text{eff}} = \rho\varepsilon$.

The stream function ψ satisfying Eq (9) is related to the velocity components by

$$\frac{1}{\rho r}\frac{\partial \psi}{\partial r} = U_z \tag{10}$$

$$-\frac{1}{\rho r}\frac{\partial \psi}{\partial z} = U_r \tag{11}$$

The vorticity of the axial flow is given by

$$\omega = \frac{\partial U_r}{\partial z} - \frac{\partial U_z}{\partial r} \tag{12}$$

from Eq (10)

$$\frac{\partial}{\partial r}(rU_z) = \frac{1}{\rho}\frac{\partial^2 \psi}{\partial r^2}$$

$$\therefore \quad \frac{\partial U_z}{\partial r} = \frac{1}{r\rho}\frac{\partial^2 \psi}{\partial r^2} - \frac{U_z}{r} \tag{13}$$

Similarly from Eq (11)

$$\frac{\partial U_r}{\partial z} = -\frac{1}{\rho r}\frac{\partial^2 \psi}{\partial z^2} \tag{14}$$

Substituting Eqs (13) and (14) in (12) yields

$$\omega = \frac{1}{\rho r}\frac{\partial^2 \psi}{\partial r^2} - \frac{U_z}{r} - \frac{1}{\rho r}\frac{\partial^2 \psi}{\partial z^2} \tag{15}$$

It is convenient to eliminate the pressure gradients from Eqs (7) and (8) above by differentiating Eq (7) with respect to r and Eq (8) with respect to z and subtract the result. Upon simplification and substitution of Eqs (10) (11) and (12) this yields:

$$r^2\left(\frac{\partial}{\partial z}\left(\frac{\omega\partial\psi}{r\,\partial r}\right) - \frac{\partial}{\partial r}\left(\frac{\omega\partial\psi}{r\,\partial z}\right)\right) - \frac{\partial}{\partial z}\left(r^3\frac{\partial}{\partial z}\left(\mu_{\text{eff}}\frac{\omega}{r}\right)\right) - \frac{\partial}{\partial r}\left(r^3\frac{\partial}{\partial r}\left(\mu_{\text{eff}}\frac{\omega}{r}\right)\right) - r\frac{\partial}{\partial z}(\rho U_\theta^2) = r^3 S_\omega \tag{16}$$

and Eq (15) also can be represented as

$$-\frac{\partial}{\partial z}\left(\frac{1}{\rho r}\frac{\partial \psi}{\partial z}\right) - \frac{\partial}{\partial r}\left(\frac{1}{\rho r}\frac{\partial \psi}{\partial r}\right) - \omega = 0 \tag{17}$$

In the present notation the equation for the swirling component may be written as

$$\frac{\partial}{\partial z}\left(rU_\theta\frac{\partial \psi}{\partial r}\right) - \frac{\partial}{\partial r}\left(rU_\theta\frac{\partial \psi}{\partial z}\right) - \frac{\partial}{\partial z}\left(r^3\mu_{\text{eff}}\frac{\partial}{\partial z}\left(\frac{U_\theta}{r}\right)\right) - \frac{\partial}{\partial r}\left(r^3\mu_{\text{eff}}\frac{\partial}{\partial r}\left(\frac{U_\theta}{r}\right)\right) = 0 \tag{18}$$

for axi-symmetric ($\partial P/\partial\theta = 0$) flows, where the source term S_ω in Eq (16) is taken to zero (see Ref 11). Inspection of Eqs (16), (17) and (18) reveals that they may be written in the general form

$$a_\phi\left\{\frac{\partial}{\partial z}\left(\phi\frac{\partial \psi}{\partial r}\right) - \frac{\partial}{\partial r}\left(\phi\frac{\phi\psi}{\partial z}\right)\right\} - \frac{\partial}{\partial z}\left\{b_\phi r\frac{\partial}{\partial z}(c_\phi\phi)\right\} - \frac{\partial}{\partial r}\left\{b_\phi r\frac{\partial}{\partial z}(c_\phi\phi)\right\} + rd_\phi = 0 \tag{19}$$

The newly introduced symbols in the basic Eq (19) are identified in Table 1.

The solution procedure developed in Gosman *et al*[11] is for 2-D axi-symmetric, general orthogonal curvilinear co-ordinates, however, upon simplification to cylindrical polar co-ordinates their general equation becomes the same as Eq (19). As a result the finite difference methods, equations and computer techniques applied in the present author's previous results[15] may be used.

Solving the basic equation

A point iterative finite difference technique is used to solve the general Eq (19). If a straightforward cylindrical polar co-ordinate system is adopted, the 'tank' illustrated below is used at the grid point *P*. (See Fig A2.)

If the above node notation is used and the difference techniques described in detail in the present author's previous results[15] are adopted, the value of a variable ϕ at an interior node p may be expressed in terms

Table 1

ϕ	a_ϕ	b_ϕ	c_ϕ	d_ϕ
ω/r	r^2	r^2	μ_{eff}	$S_\omega^0 - \frac{\partial}{\partial z}(\rho U_\theta^2)$
ψ	0	$1/\rho r^2$	1	$-\omega/r$
rU_θ	1	$\mu_{\text{eff}} r^2$	$1/r^2$	0

of the same variables at surrounding nodes thus:

$$\phi_p = \frac{\sum_{j=N,E,W,S} [D_j \phi_j] - d_{\phi p}}{\sum_{j=N,E,W,S} [D_j]} \tag{20}$$

where $\sum_{j=N,E,W,S}$ denotes summation over the surrounding nodes N, E, W and S: D_j represents the sum of the convection and dissipation terms and its evaluation is described in the appendix. Solving Eq (20) above involves assuming initial values for ϕ at each j location in the grid. The values of the source terms d_ϕ shown in Table 1 and the relevant boundary conditions are then supplied for each variable ϕ: furthermore, to effect closure an effective viscosity model must be chosen. The boundary conditions applied in this work are as depicted in Fig 1.

The form in which the finite difference approximations have been used

The above section has shown the way in which the Navier-Stokes equations in cylindrical-polar co-ordinates have been converted into finite difference approximations on the basis of an orthogonal uniform rectangular mesh system.

In the present analysis they have not been used as such. This is because we have chosen a mesh system in which the outermost mesh points lie exactly on the solid

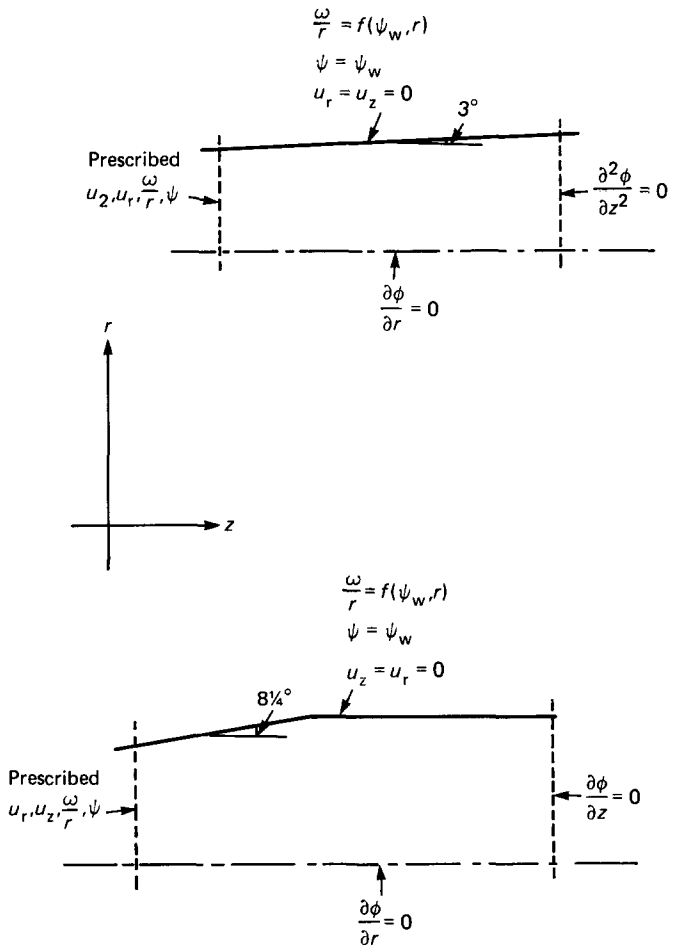

Fig 1 Boundary conditions

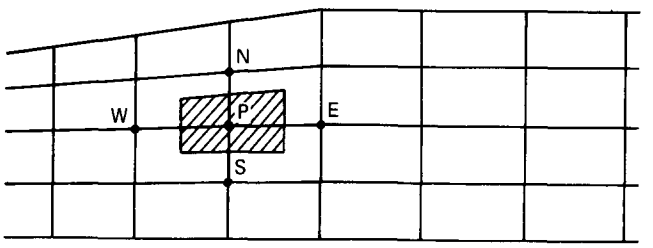

Fig 2 Typical mesh employed

boundary, and the way in which interior nodes were calculated resulted in stream-wise mesh lines slightly off-set from the horizontal, but the mesh lines in the second co-ordinate (r) remain in that direction as shown above. The difference formulae associated with a cylindrical polar system have been used at each node, which is not an exact procedure and errors are thereby incurred. To estimate the magnitude of these errors, calculations have also been performed using the Navier-Stokes equations in spherical-polar co-ordinates, for the problem of flow in the 16.5° diffuser as reported in Ref 15. The calculated results on spherical surfaces were then linearly interpolated onto the cylindrical surfaces as described above for comparison, and as expected, the discrepancy between the two approaches was found to be negligible in the cases considered, but dependent on conical angle and/or geometry curvature.

The effective viscosity model

So far it has been assumed that the effective viscosity is a calculable quantity which consists of a laminar μ, and a turbulent μ_t component. It is necessary now to assume a suitable model for μ_t. This is done by making use of Prandtl's mixing length hypothesis from which μ_t is defined as

$$\mu_t = \rho l_z^2 \frac{\partial U_z}{|\partial r|} \tag{21}$$

where l_z is the axial mixing length. It is assumed also that in the region of a solid boundary the turbulent mixing length contribution is that proposed by Van Driest[14] and modified by Patankar and Spalding[13], namely

$$l_z = 0.4y\left\{1 - \exp\left(\frac{-y\sqrt{\rho\,\tau}}{A\mu}\right)\right\} \tag{22}$$

where y is the distance from a solid boundary, τ is the local shear stress, μ the laminar viscosity and A is 26 according to Van Driest[14].

In the main regions of the flow this investigation has revealed that the mixing length distributions giving the calculations in best agreement with available experimental data are of the form

$$l_z = KR \tag{23}$$

where K is a constant and R is the radius of the flow cross-section. In this investigation, swirling flows are also considered.

The amount of swirl in a flow is hereby characterized by the swirl number S_N defined as

$$S_N = \frac{\text{Total flux of moment of momentum}}{\text{Total flux of axial momentum} \times \text{section radius}} \tag{24}$$

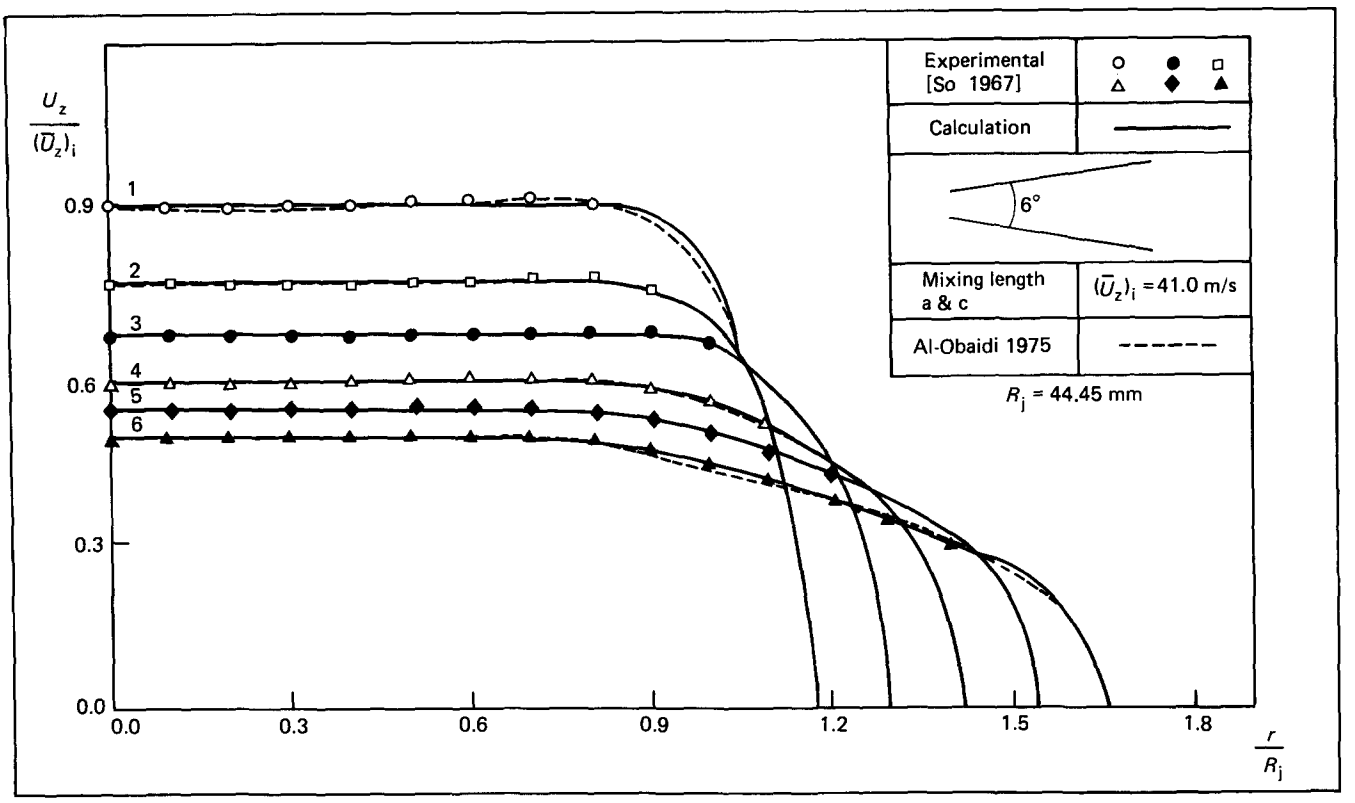

Fig 3 Axial velocity distribution: turbulent flow in 6° diffuser

This investigation was carried out for cases of swirl blade angles of 0°, 3°, 5° and 7°, but we report here only the results of swirl blade angles of 0° and 5°, for which the values of S_N were 0.0 and 0.055 respectively.

Results

As a first step, in order to test the applicability of the solution procedure discussed here, the flow in a 6° conical diffuser, studied by So[6], was calculated. All the relevant variables ϕ were assumed to have a very small initial value at each node and the boundary conditions indicated in Fig 1 were applied, some of them deduced from the experiments of So[6]. The mixing length distribution which gave the best agreement with So's data in swirl-free flow is given by:

$$l_z = 0.099R \tag{25}$$

and for swirling flow by

$$\left.\begin{aligned} l_z &= 0.099R \\ l_\theta &= 0.065R \end{aligned}\right\} \text{(see Table 2)} \tag{26}$$

In swirling flows, it was assumed that in the sublayer $l_z = l_\theta$. The axial and tangential velocity distributions are as shown in Figs 3, 4 and 5. The results of Al-Obaidi[10] who used the Patankar and Spalding[13] parabolic type of finite difference solution procedure and a Prandtl mixing length type of turbulence model are also represented in Figs 3, 4 and 5. The discrepancy observed in axial velocity profiles near the wall may be due to the approximate nature of the near-wall inlet velocity profile as there were no experimental data there, and this represents about 20% of the total flow cross-section. The tangential velocity distribution can be seen to be in excellent agreement with So's data. Note that the flow in So's diffuser was unseparated both in the absence or presence of swirl.

The calculation procedure was then applied to the problem of turbulent separated flow through a 16.5° conical diffuser. The calculations were carried out in two major stages. Each stage differed from the other as regards the forms of turbulence model used. Tables 3 and 4 summarize the various stages. The choice of model was based on whether the regions of separated* and unseparated flow can both be simultaneously predicted. It was observed that the turbulence model which predicted the existence of flow separation could not simultaneously predict the energy dissipation in good agreement with observation. However, though the simpler of the models predicted the dissipated mechanical energy in excellent agreement with the author's experiment and could not simultaneously predict flow separation, it was thought that the mechanical energy dissipation is the single property of the flow that is of greatest importance to the engineer.

The two main stages are presented viz. (1) the model which predicted the dissipated mechanical energy well and (2) the model which predicted the approximate location of the flow separation region.

Fig 6 is the axial velocity U_z distribution in swirl-free flow for the model with $l_z = 0.099R$. This shows that the outlet velocity distribution is in excellent agreement with observation despite the fact that the existence of flow separation is not predicted (see Fig 10). The dissipated energy deduced from the calculations of parts (a) of Stages 1 and 2 (Tables 3 and 4) (for 0°, 3° and 5° swirling flows) is shown in Table 5 and it can be seen that agreement with the experiment is good.

A further optimization of the axial mixing length model later revealed that a combination of $l_z = 0.099R$ and

* The location of separation was taken to be that at which the nearest grid node to the solid boundary indicated a zero axial velocity value.

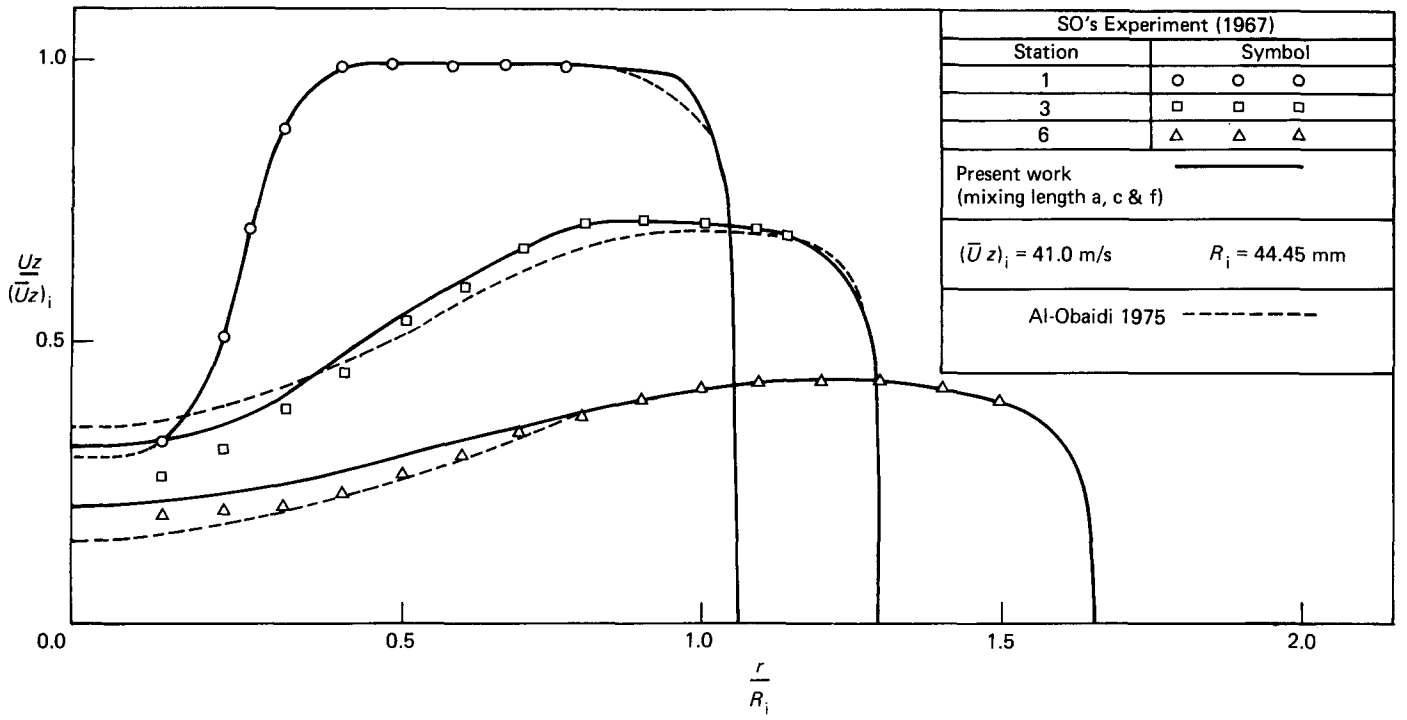

Fig 4 Axial velocity distribution (6° diffuser)

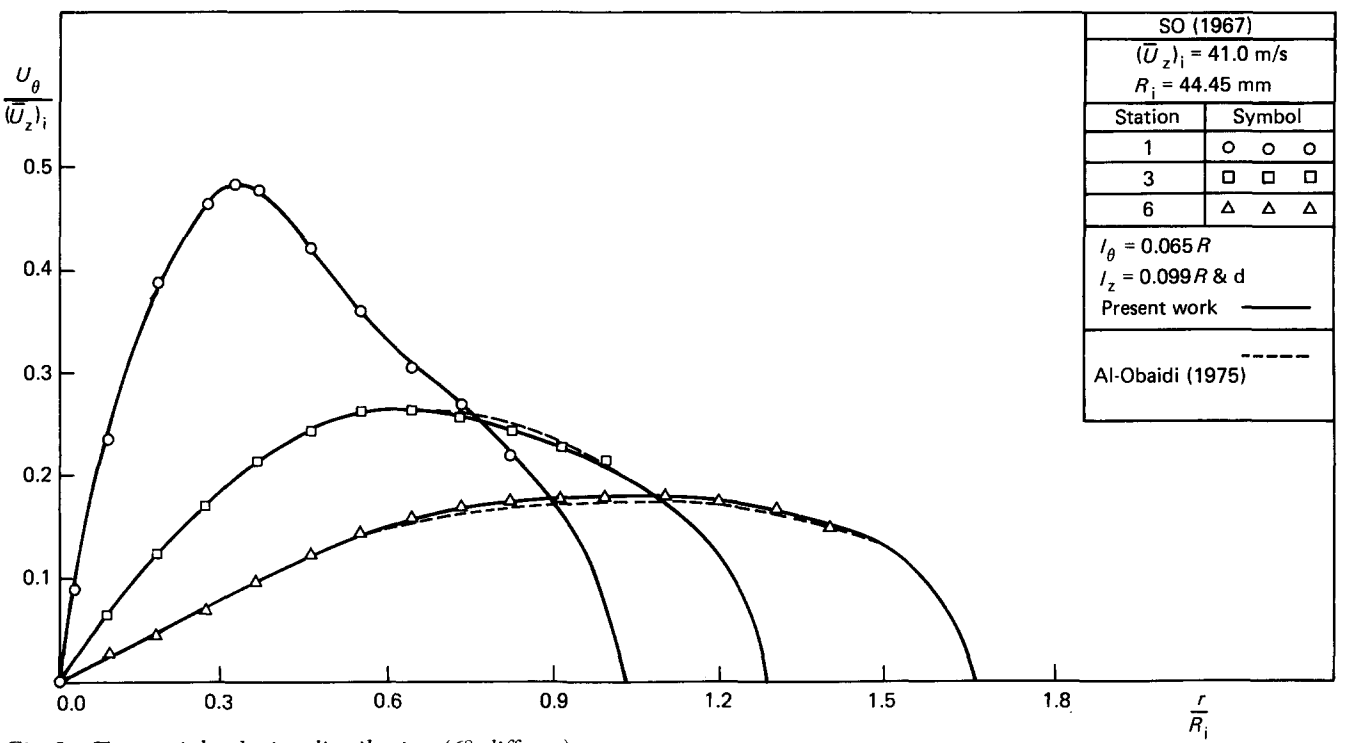

Fig 5 Tangential velocity distribution (6° diffuser)

Table 2

Diffuser angle (degrees)	Mixing length model	
	Near-wall region	Elsewhere
6 (swirl-free flow)	l_z=Van Driest law eqn (30)	$l_z=0.099R$
6 (swirling flow)	l_z=Van Driest law $l_\theta=l_z$	$l_z=0.099R$ $l_\theta=0.065R$

$l_z=0.027R$ could predict the approximate location of the experimentally observed separation zone and the dissipated energy in fair agreement with the observation, simultaneously (Fig 7). This was done by first optimizing the model to a stage where it simply predicted flow separation namely $l_z=0.027R$, and because the upstream flow is unaffected by whatever model one uses (since important velocity gradients only occur in the region governed by the near-wall model) it was convenient to start the calculation from the diffuser inlet using

Table 3

Stage 1

Diffuser angle (degrees)	Mixing length model	
	Near-wall region	Elsewhere
16.5 (swirl-free flow)	l_z=Van Driest law	(a) $l_z=0.099R$ (b) $l_z=0.099R$ $l_z=0.027R$

Table 4

Stage 2

Diffuser angle (degrees)	Mixing length model	
	Near-wall region	Elsewhere
16.5 (swirling flow)	l_z=Van Driest law	(a) $l_z=0.099R$ $l_\theta=0.065R$ (b) $l_z=0.099R$ $l_z=0.027R$ $l_\theta=0.065R$

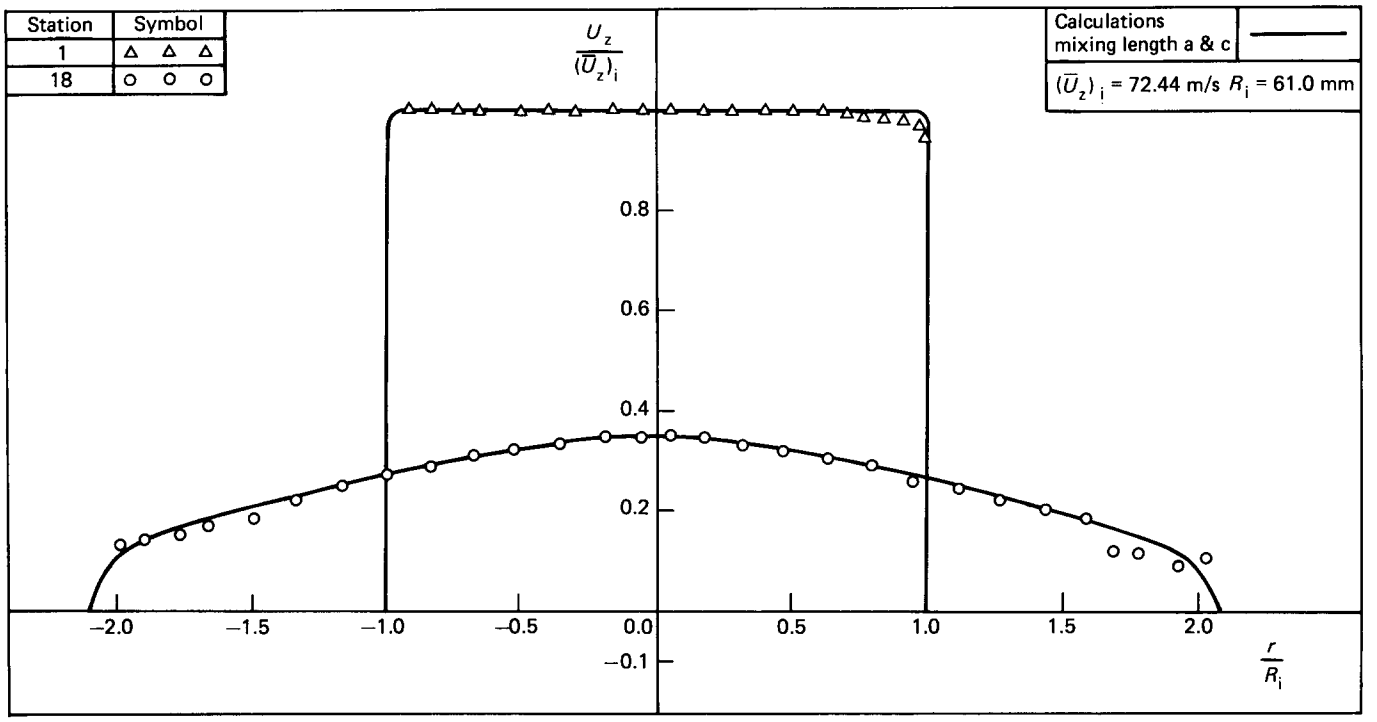

Fig 6 Axial velocity distribution (16.5° diffuser)

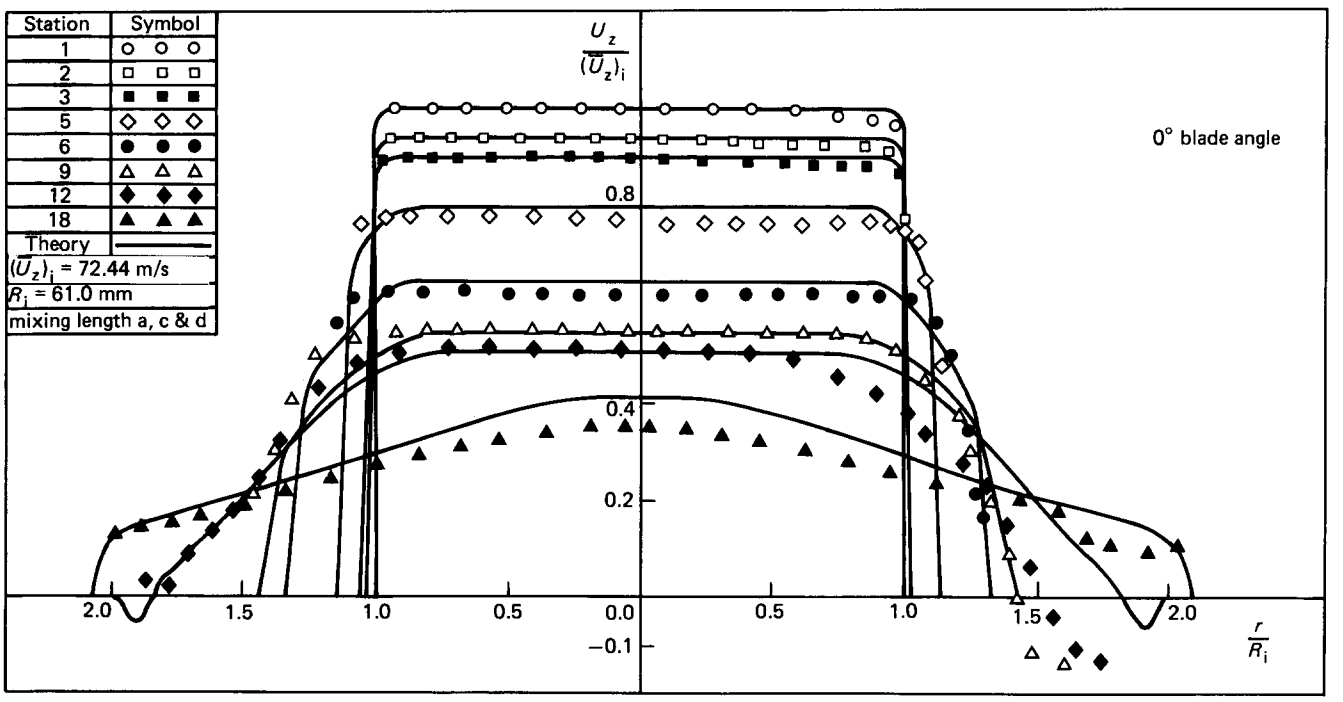

Fig 7 Axial velocity distribution (16.5° diffuser)

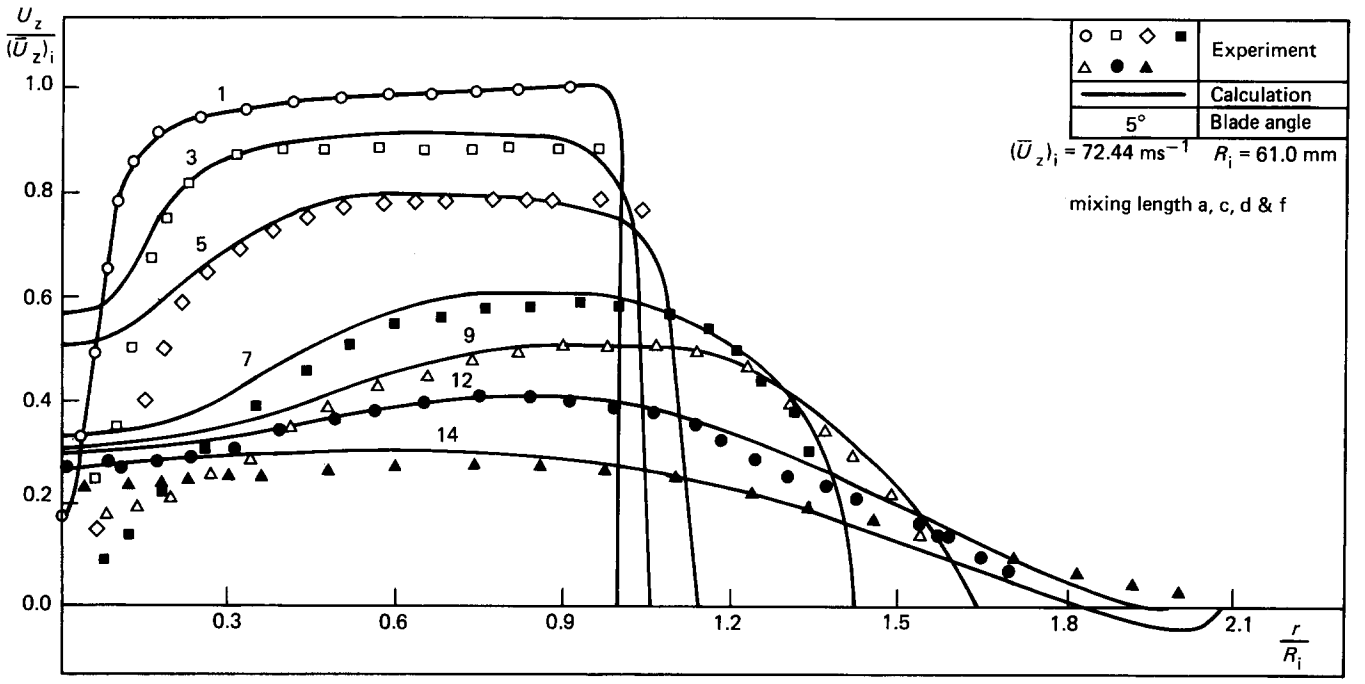

Fig 8 Axial velocity distribution (16.5° diffuser)

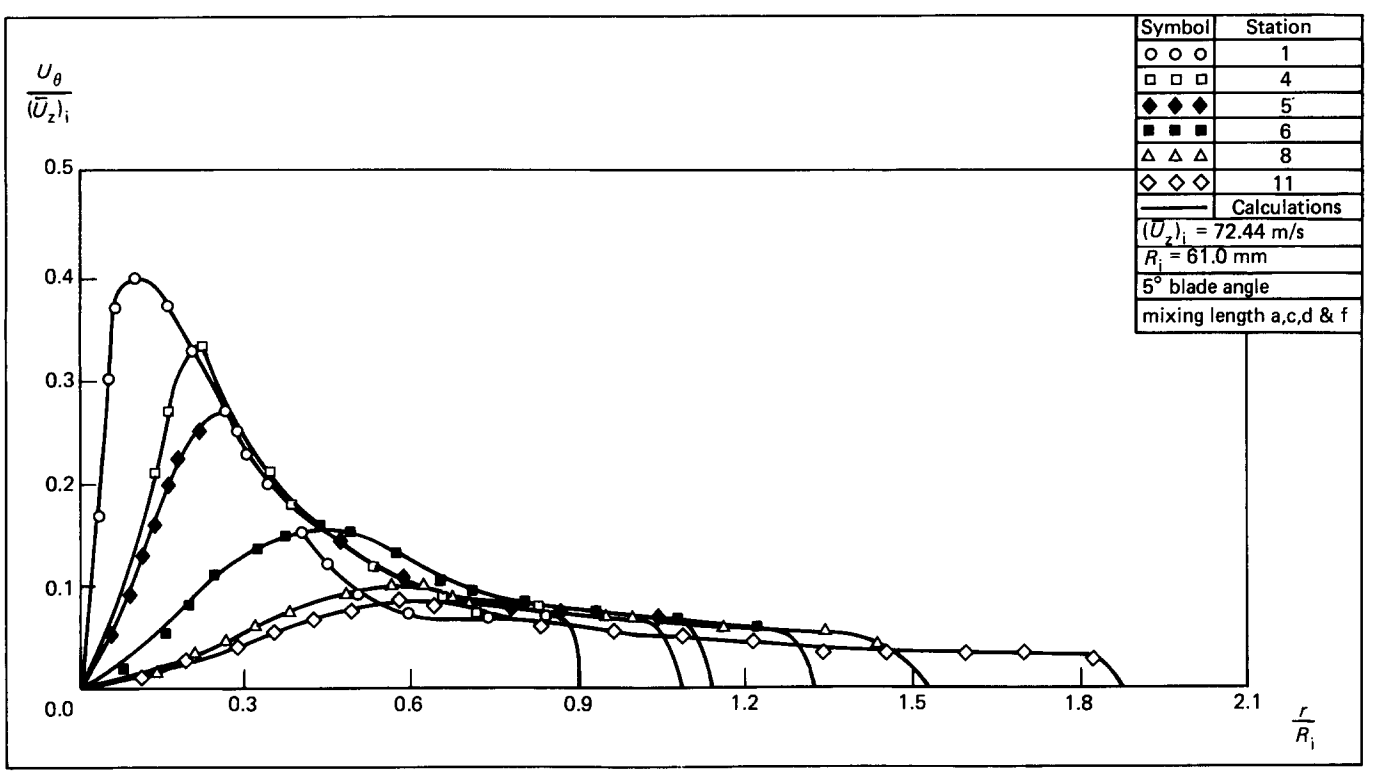

Fig 9 Tangential velocity distribution (16.5° diffuser)

$l_z = 0.099R$ and change over to $l_z = 0.027R$ and then back to $l_z = 0.099R$ within the tailpipe. The predicted dissipative losses were not quite as well predicted as when $l_z = 0.099R$ alone was used, but were observed to be about 20% different from those measured. The axial velocity distribution, Fig 7 shows the occurrence of flow separation within the observed region, but the profiles in general are not so well predicted. The tangential model $l_\theta = 0.065R$ was then super-imposed on this final axial mixing length model, and the results of Fig 9 show that the tangential velocity distribution is in good agreement with the observation. That this is the case despite the poorer agreement in the axial velocity distribution, Fig 8 demonstrates that a change in the distribution of one component of velocity brought about by a change in the corresponding mixing length model has little or no effect on the distribution of the other velocity component.

The centre-line and near-wall axial velocity distributions for the main stages of the calculation are also shown in Figs 10 and 11. Fig 12 is a graphical representation of the final mixing length models used in this investigation.

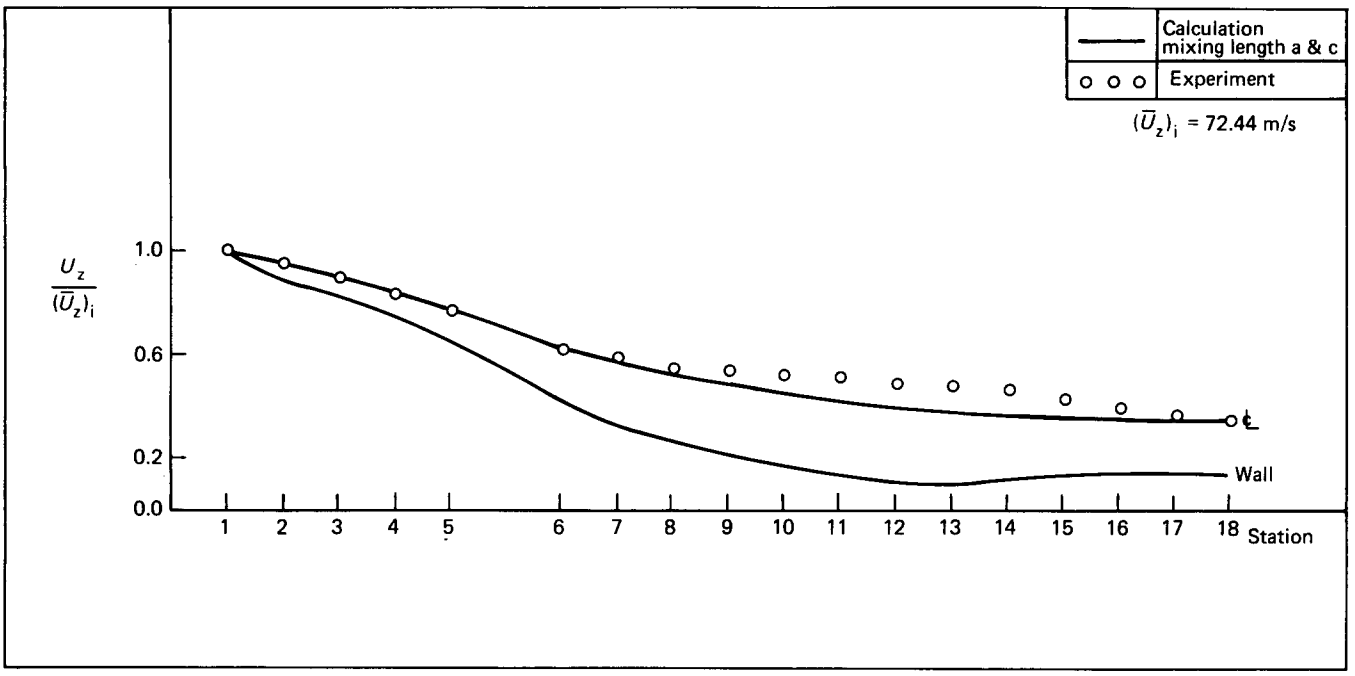

Fig 10 Centre-line and near wall axial velocity (16.5° diffuser)

Table 5

Blade angle	$L_{0\text{-}1}$	$L_{1\text{-}2}$	C_{PR}	$L_{1\text{-}2}$
(degrees)	% of $\int_1 \frac{U^2}{2}\,d\dot{m}$ (EXPTL)	% of $\int_1 \frac{U^2}{2}\,d\dot{m}$ (EXPTL)	% (EXPTL)	% (CALC)
0	0.8	23.4	75.0	23.6
3	1.3	17.34	79.0	16.2
5	2.4	15.8	80.82	15.2
7	2.7	19.35	77.66	–

Where by applying the steady flow energy equation at sections 0, 1 and 2:

$L_{0\text{-}1}$ = swirl generator loss

$$\int_0 \left(\frac{P_g}{\rho}+\frac{U^2}{2}\right)d\dot{m}-\int_1 \left(\frac{P_g}{\rho}+\frac{U^2}{2}\right)d\dot{m} \tag{26a}$$

$L_{1\text{-}2}$ = dissipation in diffuser

$$\int_1 \left(\frac{P_g}{\rho}+\frac{U^2}{2}\right)d\dot{m}-\int_2 \left(\frac{P_g}{\rho}+\frac{U^2}{2}\right)d\dot{m} \tag{26b}$$

C_{PR} = pressure recovery coefficient

$$\frac{\int_1 (P_g/\rho)\,d\dot{m}-\int_2 (P_g/\rho)\,d\dot{m}}{\int_1 (U^2/2)\,d\dot{m}} \tag{26c}$$

C_{PR_I} = inviscid pressure recovery coefficient

$$1-\left(\frac{A_1}{A_2}\right)^2 = 95\% \tag{26d}$$

Deductions

The results of the calculation of the flow distribution and dissipative losses in conical diffusers have been compared in this paper with the experimental data, and the main deductions fall into the following categories:

1) For the case of non-swirling, unseparated diffuser flow, the mixing length distribution finally adopted as giving the predicted flow distribution in best agreement with experimental data is given by

$$l_z = 0.099R \tag{27}$$

2) For the case of non-swirling, separated diffuser flow, the finally adopted mixing length distribution $l_z = 0.099R$ for non-swirling unseparated flow predicted the dissipative losses in the 16.5° angle diffuser-tailpipe assembly in excellent agreement with observation. However, the observation was that the same mixing length ($l_z = 0.099R$) could not predict the occurrence of flow separation. For the prediction of flow separation, it was necessary to change from Eq (27) to the equation

$$l_z = 0.027R \tag{28}$$

as the flow developed, and the quality of the predicted dissipative losses resulting was poorer than for those resulting from the distribution described by Eq (27) acting alone.

3) For the case of swirling, unseparated flow, the axial mixing length distribution Eq (27) above was retained and the tangential mixing length distribution which was adopted as giving the best agreement for both the distribution of tangential velocity and the dissipative losses in the 16.5° angle diffuser-tailpipe assembly was given by

$$l_\theta = 0.065R \tag{29}$$

It was observed that the changes in the distribution of one component of velocity brought about by a change in the corresponding mixing length distribution, had little or no

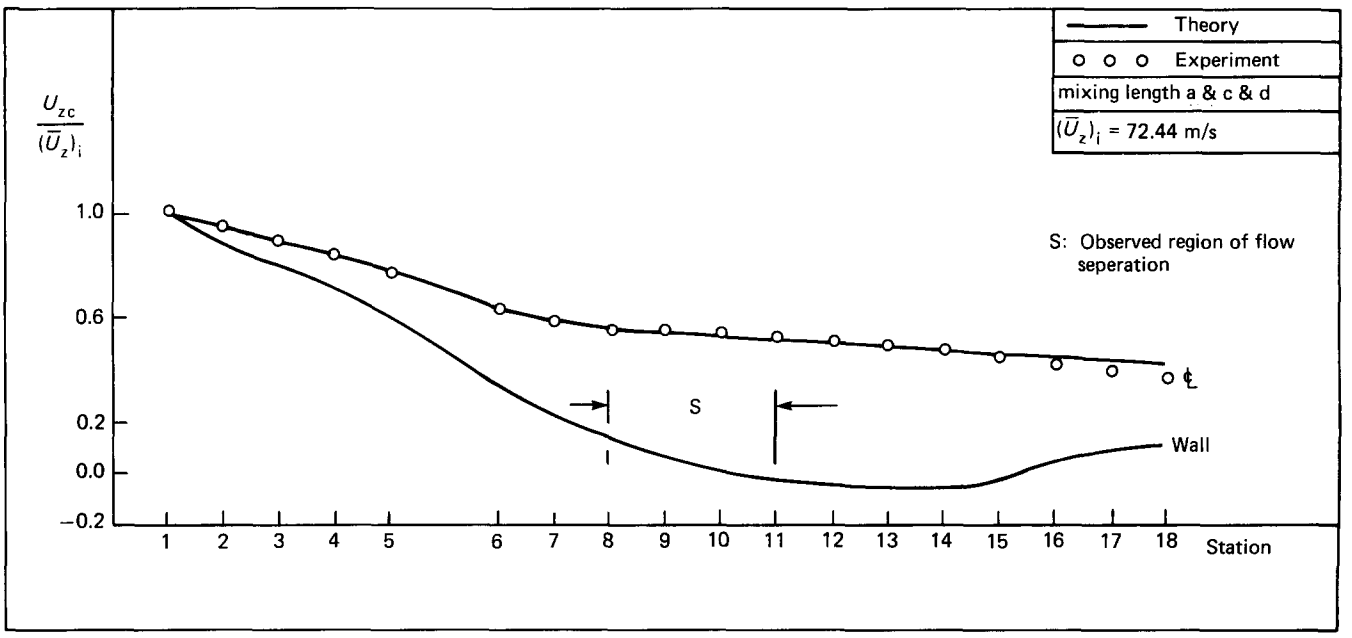

Fig 11 Axial centre-line and near-wall velocity (16.5° diffuser)

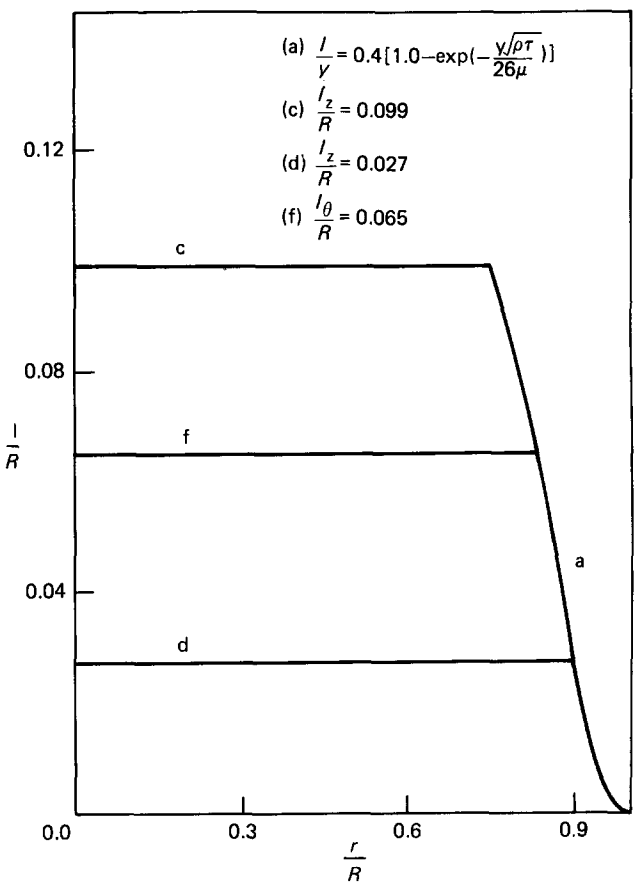

Fig 12 Mixing length distribution (present work)

effect on the distribution of the other component of velocity.

4) For the case of swirling, separated flow, the finally adopted axial and tangential mixing length distributions represented by Eqs (27) and (29) combined, were observed to predict both the tangential velocities and the dissipative losses in the 16.5° angle diffuser-tailpipe assembly in good agreement with observation. However, though to predict the occurrence of flow separation and the dissipative losses in fair agreement with observation, the tangential model (for which the tangential flow distribution quality of (2) above was retained) was unchanged, a change-over from axial distribution Eq (27) to (28) was also necessary. The prediction of the axial flow distribution for the cases of the change-over type of calculations was better than for those which employed Eq (27) alone.

The Patankar and Spalding modification of the Van Driest hypothesis given by

$$l_z = l_\theta = 0.41y\left\{1-\exp\left(\frac{-y\sqrt{\tau\rho}}{26\mu}\right)\right\} \tag{30}$$

was adopted throughout in the immediate vicinity of the solid boundary. Its detailed effects on the near-wall separation region are still undergoing tests.

Conclusions

The following paragraphs form the main conclusions of the investigations reported here:

(1) The time-mean flow distribution in pipes and diffusers can be calculated by applying suitable adaptations of the Gosman *et al*[11] finite difference method of solution of the full Navier-Stokes equations.

(2) Simple forms of the Prandt mixing length model of turbulence have evolved which can be adapted to the problems of the time-mean unseparated and separated, non-swirling and swirling flows.

(3) It has been noted that the mixing length distribution which predicted the dissipated mechanical energy in good agreement with the experimental data could not simultaneously calculate the occurrence of flow separation. More involved mixing length distributions calculated the extent and approximate location of the regions of flow separation and reattachment.

(4) Arising from the previous three conclusions, it now seems possible that a reliable prediction of the time-mean flow distribution and the associated dissipative losses in wide angle conical diffusers similar to those investigated here can be obtained.

(5) This investigation has shown that the mixing length turbulence models are useful and are worth improving upon. The complexity and costs given rise to by other more sophisticated models, which do not necessarily yield the best results in the same situation, provide a powerful incentive to continue to exploit the simplicity of the mixing length hypothesis.
(6) Finally, it can be observed that the asymmetry of the flow distribution in wide angle diffusers resulting from the large regions of stall, cannot be accurately predicted by the theory reported in this work.

Appendix

In order to evaluate the term D_j of Eq (20) for all j the following expressions have been used:

$$D_j=\{A'_j+C_{\phi j}(b_{\phi,j}+b_{\phi,p})B'_j\} \qquad j=\mathrm{N,S,W,E} \tag{A1}$$

where

$$A'_j=\frac{A_j}{V_p} \tag{A2}$$

and

$$B'_j=\frac{B_j}{V_p(b\phi,j+b_{\phi,p})} \tag{A3}$$

$$A_S\equiv a_{\phi,p}(\psi_{sw}-\psi_{se}) \tag{A4}$$

$$A_W\equiv a_{\phi,p}(\psi_{nw}-\psi_{sw}) \tag{A5}$$

$$A_w\equiv a_{\phi,p}(\psi_{nw}-\psi_{sw}) \tag{A6}$$

$$A_E\equiv a_{\phi,p}(\psi_{se}-\psi_{ne}) \tag{A7}$$

$$B_N=\frac{b_{\phi,N}+b\phi_p}{8}\frac{z_E-z_W}{r_N-r_p}(r_N+r_p) \tag{A8}$$

$$B_S=\frac{b_{\phi,S}+b\phi_p}{8}\frac{z_E-z_W}{r_p-r_S}(r_S+r_p) \tag{A9}$$

$$B_W=\frac{b_{\phi,W}+b\phi_p}{8}\frac{r_N-r_S}{z_p-z_W}(r_W+r_p) \tag{A10}$$

$$B_E=\frac{b_{\phi,E}+b\phi_p}{8}\frac{r_N-r_S}{z_E-z_p}(r_E-r_p) \tag{A11}$$

$$V_p=\frac{r_p}{4}(z_E-z_W)(r_N-r_S) \tag{A12}$$

The nodal subscripts N, S, W, E, ne, nw, se and sw which surround the node p are shown in Fig A1.

The calculations of flow in conical diffusers with tailpipes presented in the main body of this article based on the time-averaged Navier-Stokes equations, used cylindrical-polar coordinates with finite-difference expressions appropriate to a rectangular mesh system. In order to place mesh points on the conical boundary, the mesh actually used was non-orthogonal, as shown in Fig A2, and that procedure involved some degree of approximation.

Various alternatives exist for the choice of co-ordinate system and mesh arrangement for the configuration studied.

The first possibility would be to use a cylindrical-polar co-ordinate system with a rectangular grid, and to use one of the standard procedures for dealing with boundary points which do not coincide with mesh points. However, this procedure tends to be unsatisfactory because one (or more) boundary points almost inevitably lies close to, but not on, a mesh point leading to large discretization errors.

A second alternative would be to use a co-ordinate system locally appropriate to the geometry. That is, spherical co-ordinates would be used in the conical diffuser, changing to a cylindrical system in the tailpipe. However, this would be rather cumbersome and it might be difficult to ensure a smooth change-over. There would also be the practical difficulty of comparing experimental results obtained along plane sections normal to the axis, with results calculated along spherical surfaces.

A third alternative would be to use a form of co-ordinate transformation which maps the physical domain onto a cylinder, and then to solve the equations using cylindrical polar co-ordinates with a rectangular mesh in the transformed plane. This would considerably complicate the form of the equations and might lead to computational difficulties.

Instead of these possible approaches, we have directly applied the discretized Navier-Stokes equations in cylindrical-polar co-ordinates formulated on the basis of a rectangular mesh system to the problem in a local rhombic mesh system as shown in Fig A2.

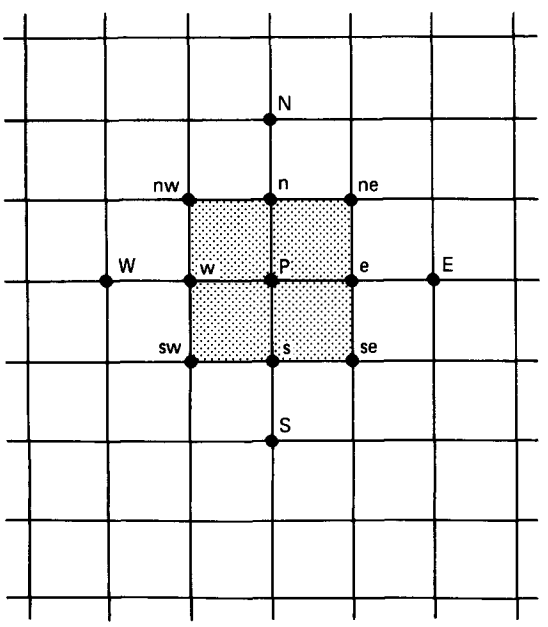

Fig A1 The nodal subscripts which surround the node P

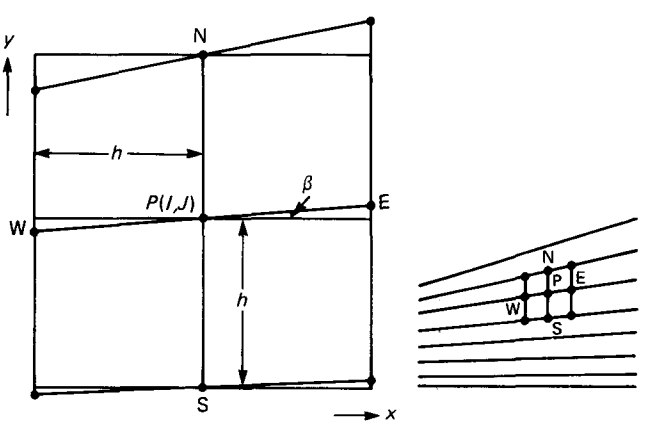

Fig A2 Deformed rectangular mesh

By applying the discretized Navier-Stokes equations in cylindrical polar co-ordinates directly onto this distorted grid system, it was observed[15] that the errors incurred were negligible.

It should however be clearly stated that this approach is only approximate.

It is interesting to note that Marsh[16] in his investigation on an arbitrary turbomachine has used a slightly different finite difference scheme in which in order to maintain an overall accuracy of the second order or higher in the local spacing of the distorted grid points in the cross-stream direction which he denoted by K_0, he obtained the finite difference approximations by using the function values at ten specially selected grid points. His more accurate approach would therefore have taken into account the smaller terms which the present authors have taken as small and negligible.

References

1. **Furuya Y., Sato, T. and Kushida T.** The loss of flow in conical diffusers with suction at the entrance. *J.S.M.E., 1966*, **9**(*33*), *131–137*
2. **Duggins, R. K., Lampard D. and Sanders A. T.** Further investigation of conical diffusers with annular injection. *J. Mech. Eng. Sci., 1978*, **20**(*1*), *58–64*
3. **Senoo Y. and Nishi M.** Improvement of the performance of conical diffusers by vortex generators. *Trans. A.S.M.E., 1974, 4–15*
4. **Cochran D. L. and Kline S. J.** The use of short flat vanes as a means of producing efficient wide-angle two-dimensional subsonic diffusers. *N.A.C.A. Report TN -4309, 1959*
5. **Turner J. T.** Improvement of wide-angle conical diffusers performance by means of conical vanes. *Symposium on internal flows, Salford University, 1971*
6. **So K. L.** Vortex phenomenon in a conical diffuser. *A.I.A.A.J., 1967*, **5**(*6*), *1072–1078*
7. **Cockrell D. J. and Kline A. L.** A review of literature on subsonic fluid flow through diffusers. *B.H.R.A., TN. 902, 1967*
8. **McDonald A. T., Fox R. W. and Van Dewoestine R. V.** Effects of swirling inlet flow on pressure recovery in conical diffusers. *A.I.A.A.J., 1971*, **9**(*10*), *2014–2018*
9. **Goldstein S.** Modern development in fluid dynamics, *Clarendon Press, Oxford, 1938*
10. **Al-Obaidi S. H. R.** Swirling flow in conical diffusers, *Ph.D. Thesis, London University, 1975*
11. **Gosman A. D., Pun W. M., Runchal A. K., Spalding D. B. and Wolfstein M.** Heat and mass transfer in recirculating flows. *Academic Press, London and N.Y., 1969*
12. **Launder B. E. and Spalding D. B.** Mathematical models of turbulence. *Academic Press, London and N.Y., 1972*
13. **Patankar S. V. and Spalding D. B.** Heat and mass transfer in boundary layer. *Intertex Books, London, 1970*
14. **Van Driest E. E.** On turbulent flow near a wall. *J. Aero. Sci., 1956*, **23**, *1007*
15. **Okhio C. B.** Swirling flow through conical diffusers. *Ph.D. Thesis, London University, 1981*
16. **Marsh H.** A digital computer program for the through-flow fluid mechanics in an arbitrary turbomachine using a matrix method. *Aero. R.C., R & M. No. 3509, July, 1966*